Assessment of Acute Antivascular Effects of Vandetanib with High-Resolution Dynamic Contrast-Enhanced Computed Tomographic Imaging in a Human Colon Tumor Xenograft Model in the Nude Rat[1]

Joo Ho Tai[*,†], Jean Tessier[‡], Anderson J. Ryan[‡], Lisa Hoffman[*], Xiaogang Chen[†] and Ting-Yim Lee[*,†,§]

[*]Lawson Health Research Institute, St Joseph's Health Care London, London, Ontario, Canada; [†]Imaging Research Laboratories, Robarts Research Institute, the University of Western Ontario, London, Ontario, Canada; [‡]AstraZeneca, Alderley Park, Macclesfield, Cheshire, United Kingdom; [§]Department of Medical Biophysics and Medical Imaging, Schulich School of Medicine and Dentistry, the University of Western Ontario, London, Ontario, Canada

Abstract

Tumor size is not a reliable marker for the assessment of early antivascular effects of antiangiogenics. In the present study, we used 200-μm in-plane high-resolution dynamic contrast-enhanced computed tomography (DCE-CT) to non-invasively assess the immediate antivascular effects of vandetanib in a subcutaneous human colon cancer (LoVo) xenograft model in nude rats and to investigate correlation between changes in CT perfusion parameters and tumor volume or immunohistochemical end points. At 3 to 4 weeks after LoVo cell implantation, the animal was gavaged with either vandetanib (50 mg/kg) or vehicle twice (22 hours apart) and scanned with a preclinical DCE-CT scanner before (0 hour) and after treatment (24 hours). Quantitative maps of blood flow (BF) and volume (BV) of the tumor were calculated from the acquired DCE-CT images. The rats were divided into nonhypovascular, hypovascular, and combined (regardless of vascularity) groups. In the nonhypovascular group, significant decreases in both tumor BF and BV were observed in the vandetanib-treated rats compared with increases in the vehicle-treated rats. A significant decrease in BV was detected in the vandetanib-treated rats in the combined group as well. No differences in tumor growth, vascular endothelial growth factor expression, microvessel density, or apoptosis were observed between vandetanib- and vehicle-treated rats in all three groups. These results demonstrate that BF and BV imaging biomarkers from DCE-CT imaging can be used for rapid monitoring of immediate (24 hours after) antimicrovascular effects of vandetanib on tumors, even in the absence of significant changes of tumor volume or clinically relevant immunohistochemical end points.

Neoplasia (2010) 12, 697–707

Introduction

A rapid phase of tumor growth occurs when a tumor switches to an angiogenic phenotype [1,2]. Tumor angiogenesis—the formation of new blood vessels from existing blood vessels—is initiated by the secretion of various growth factors from tumor cells and the surrounding stroma [3]. Among the many proangiogenic growth factors, vascular endothelial growth factor (VEGF) plays a pivotal rate-limiting role in the angiogenic cascade, enhancing endothelial cell (EC) survival, proliferation, invasion, migration, and capillary tube formation as well as permeability of the endothelium [4,5]. Overexpression of VEGF correlates with increased tumor growth rate, microvessel density (MVD), tumor metastatic potential, and poor prognosis in a variety of malignancies [6].

Vandetanib (AstraZeneca, Macclesfield, UK) is an orally bioavailable inhibitor of VEGF receptor (VEGFR) 2 tyrosine kinase (TK) activity [7] that has been shown to block tumor-induced angiogenesis through inhibition of VEGF-induced signaling in ECs in human tumor xenografts [8–10]. In addition to VEGF signaling inhibition, vandetanib also inhibits epidermal growth factor receptor TK, although this activity is not considered essential for antitumor activity *in vivo* because vandetanib has been shown to inhibit tumor growth in a dose-dependent manner in a histologically diverse panel of human tumor xenografts including tumor models that do not respond to gefitinib, a highly selective epidermal growth factor receptor TK inhibitor [7].

Clinical evaluation of treatment responses relies largely on measurements of tumor size formalized in 1981 as the World Health Organization criteria [11] and in 2000 as the Response Evaluation Criteria in Solid Tumors (RECIST) [12] and this was revised in 2009 [13]. Typically, serial tumor size assessments are performed several weeks/months after the drug treatment course/cycle has been started. However, a considerable amount of functional information may be gained by observing early changes in imaging biomarkers. Furthermore, with the advent of molecular biology, the focus of drug development has shifted from cytotoxic chemotherapies to the development of molecular targeted therapies. Many of these new therapies are expected to be primarily cytostatic in action, making traditional tumor size response criteria less appropriate for early assessment of drug efficacy. For drugs targeting tumor vasculature, several tumor biomarkers have been suggested. For example, MVD has been shown to correlate with tumor growth, tumor metastasis, and patient prognosis [14–16]. However, because tumor biopsy is an invasive procedure that is sensitive to sampling variability because of the underlying heterogeneity of the tumor, it may not be a preferred option for longitudinal patient monitoring [17]. Thus, there is a need for the development of noninvasive methods, such as imaging, that are able to monitor tumor response to antivascular therapies while potentially providing a better assessment of the response of the whole tumor [18,19].

Dynamic contrast-enhanced magnetic resonance imaging (DCE-MRI) has been used extensively in preclinical and clinical settings to monitor the effect of VEGF signaling inhibitors or vascular disrupting agents by providing evidence of drug activity on tumor haemodynamics [20,21], but the practical implementations are not straightforward and the various analysis strategies used can have considerable consequences on both the values and the interpretation of the derived parameters [22].

Dynamic contrast-enhanced computed tomography (DCE-CT) has also been developed recently as a noninvasive *in vivo* imaging method to investigate tumor-associated vasculature [23]. The technique benefits from the linear relationship between contrast concentration in both tissue and blood and image intensity that simplifies modeling to determine tumor blood flow (BF), blood volume (BV), mean transit time, and vascular permeability [24,25]. Furthermore, wide availability of clinical CT scanners, easy implementation of study protocol, and commercially availability of analysis software have resulted in an increasing use of DCE-CT to study angiogenesis [26,27] in a variety of cancers and their response to antiangiogenesis therapy and chemo/radiotherapy in patients [28–30]. Despite this, owing to the limited availability of preclinical (small animal) CT scanners, DCE-CT has not been used as extensively as DCE-MRI in testing the effects of antiangiogenics on tumor vasculature in rodent tumor models.

In the present study, we report the immediate (24 hours) effects of vandetanib treatment on tumor vasculature measured noninvasively using quantitative DCE-CT in the LoVo human colon tumor xenograft model in nude rats with a dedicated high-resolution (200-μm in-plane resolution) small animal CT scanner.

Materials and Methods

Drugs Preparation

Clinical grade vandetanib was provided by AstraZeneca. Vandetanib was suspended in 1% (vol./vol.) Tween 80 (Sigma, Oakville, Ontario, Canada) by gentle milling with equal volume of 6-mm solid glass beads (Kimble Kontes LLC, Sigma) overnight on blood tube rotator (American Hospital Supply Corp, Miami, FL) at room temperature, and the suspension was used within 48 hours of preparation. Vandetanib was administered as a homogeneous suspension by oral gavage at a dosage of 50 mg/kg body weight.

Cell Culture

The LoVo human colon adenocarcinoma cell line (no. CCL-229; ATCC, Manassas, VA) was purchased and maintained in F12K growth medium (Gibco, Burlington, Ontario, Canada), supplemented with 10% fetal bovine serum. Cells were typically passaged twice a week and were expanded appropriately to yield enough cells to be implanted into nude rats.

Animals and Tumor Xenograft Model

All experimental procedures were approved by our institutional research ethics board. Four- to six-week-old male athymic nude rats (Crl:NIH-rnu) were purchased from Charles River Laboratories (Wilmington, MA). The rats were caged in groups of two and fed with standard rodent chow and water *ad libitum*. On the day of implant, the LoVo cells were washed with Hank's balanced salt solution (Sigma), trypsinized using 0.25% Trypsin-EDTA (Sigma), resuspended in growth medium to neutralize the trypsin, and centrifuged at 600 rpm for 5 minutes to pellet the cells. Cells were then resuspended at a concentration of 10^8 cells/ml in serum-free F12K medium with penicillin (100 U/ml) and streptomycin (100 μl/ml) added. One hundred fifty microliters of this cell suspension (1.5 × 10^7 cells/rat) was implanted subcutaneously into the left flank of each nude rat.

Functional DCE-CT Protocol, Schedule of Vandetanib Dosing, and Blood Collection

Functional DCE-CT imaging was carried out 3 to 4 weeks after tumor cell transplantation. Inhalation anesthesia in each animal was induced and maintained with a mixture of oxygen and 0.75% to 1.5% isoflurane administered through a nose cone. A 23-gauge angiocatheter was placed in a tail vein for subsequent contrast injection.

All imaging was performed with a GE Healthcare eXplore Ultra small animal CT scanner (London, Ontario, Canada). The CT scanner is capable of fast rotation speed and collects a complete 360° projection data set every second for reconstruction into forty-five 0.9-mm-thick slices covering an axial distance of 4.05 cm. The in-plane resolution of the CT images is 200 μm (*vs* ~750 μm of clinical CT images). An anteroposterior radiography (scout scan) of the rat was performed to enable selection of the scan limits for the DCE-CT scanning of the whole tumor. The DCE-CT scanning consisted of two phases: in the first phase, the tumor was scanned every second for 30 seconds using

an x-ray tube voltage of 80 kV(peak) and a tube current of 60 mA and a 1-second gantry rotation time; the second phase was delayed by 10 seconds from the first phase in which the tumor was scanned once every 10 seconds for 150 seconds using the same tube voltage and current. Nonionic contrast (Omnipaque 300; GE Healthcare, Piscataway, NJ) at the dosage of 2.2 µl/g (1.7 mmol/kg body weight) was injected using an infusion pump through the tail vein catheter during 5.0 to 5.8 seconds followed by 0.5 ml of saline injected for 3.8 seconds. The infusion pump was triggered 5 seconds into the DCE-CT scanning.

After the first DCE-CT scanning, the vandetanib treatment group ($n = 13$) was given vandetanib (50 mg/kg) by oral gavage, and the control group ($n = 8$) was given the vehicle (1% Tween 80). At 22 hours after the first dose, rats were given a second dose of vandetanib or vehicle by oral gavage. At 24 hours after the first dose, all rats were DCE-CT scanned again.

Before the first dose of vandetanib and immediately after the DCE-CT scan after the second dose of vandetanib, blood was collected from the tail vein catheter and plasma was separated for the measurement of vandetanib concentration. All rats were killed after the second DCE-CT scan, and blood was collected by intracardiac injection of potassium chloride. Within 15 to 20 minutes, tumors were excised and cut into thin (2-3 mm) slices. The slices were fixed in 10% buffered formalin for 48 hours before being processed for paraffin embedding.

Measurement of Perfusion Parameters: Hypovascular and Nonhypovascular Groups

The acquired DCE-CT scanning data were reconstructed with a cone-beam filtered back-projection algorithm into 45 volumes of forty-six 512 × 512 images each for a total of 2070 images. For each transverse slice through the tumor, we obtained 45 dynamic images distributed during the 3-minute scanning time, and the nominal size of each image voxel was $0.2 \times 0.2 \times 0.9$ mm^3. The reconstructed images were transferred to an Advantage Window workstation (GE Healthcare) and maps of the absolute value of four perfusion parameters in the tumor—BF (ml/min per 100 g), BV (ml/100 g), mean transit time (MTT; second), and permeability surface area product (PS; ml/min per 100 g)—were generated using CT Perfusion 4 (GE Healthcare) developed in our laboratory [23]. A 2 × 2-pixel region of interest (ROI) was placed within the aorta to determine the artery concentration *versus* time curve, which is needed to calibrate (deconvolve) the tumor contrast concentration curve for the calculation of perfusion parameters [23].

For each slice, the tumor ROI was defined using an average contrast-enhanced image, which was generated by averaging all the dynamic images. The quantitative values of each perfusion parameter in all tumor ROIs were divided into bins, and the number of pixels in each bin was expressed as a percentage of the total number of pixels in the whole tumor to arrive at the normalized histogram of the perfusion parameter. The mean value of each perfusion parameter in the whole tumor was obtained as the first moment of the normalized histogram. Tumor volume (TV) was calculated by multiplying the total number of pixels in the whole tumor by the pixel volume 0.2 mm (x) × 0.2 mm (y) × 0.9 mm (z) = 0.036 mm^3. The percentage change in TV after vandetanib or vehicle treatment was calculated from the following formula: [(1 − TV after treatment) / TV before treatment] × 100.

The presence or absence of a hypovascular core in every tumor was examined and confirmed using the CT perfusion maps generated from the first scan. A hypovascular tumor was defined as follows: at least one image slice (thickness; 0.9 mm) from the whole TV showed a tumor core with an area greater than 10% of the tumor area and a mean BF less than 75% of that measured in the left and right erector spinal muscles. Any rat bearing a hypovascular tumor xenograft as defined above was assigned to the hypovascular group ($n = 12$), and those without were assigned to the nonhypovascular group ($n = 9$). In the nonhypovascular group, five were treated with vandetanib and four were treated with vehicle, whereas in the hypovascular group, eight were treated with vandetanib and four were treated with vehicle, respectively.

Measurement of Plasma Concentration for Vandetanib

Plasma concentrations of vandetanib was determined by reverse-phase high-performance liquid chromatography with tandem mass spectrometry as previously described [31]. The calibration range for vandetanib was from 5.0 to 1000 ng/ml.

Immunohistochemistry and Image Analysis

The paraffin-embedded tumor samples were cut into 3- to 5-µm-thick sections. For VEGF staining, two sequential sections were both placed on the same slide; one section for VEGF staining and another for negative control staining by omitting the primary antibody. After overnight incubation at 4°C with the primary antibody that is mouse monoclonal to VEGF (1:50 dilution; Abcam, Cambridge, MA), sections were washed and treated with a secondary biotinylated horse anti-mouse IgG antibody (1:200 dilution; Vectastain avidin-biotin complex method kit; Vector Laboratories, Burlingame, CA), washed again, exposed to avidin-conjugated horseradish peroxidase H complex, and incubated in diaminobenzidine and hydrogen peroxide. The slides were then mounted for image analysis of VEGF expression. For image analysis, each slide with two sequential tumor sections, one of VEGF and one of negative control staining, was scanned with an Aperio ScanScope CS scanner (Aperio Technologies, Inc, Vista, CA) at 20×. Using the Image J program (Image J 1.41o; National Institutes of Health, Bethesda, MD; http://rsb.info.nih.gov/ij), the pixel intensity of the ScanScope image was inverted, and a ROI was drawn around the entire tumor area in the VEGF-stained section for the calculation of the mean pixel intensity of VEGF expression. To minimize the effect of nonspecific VEGF expression/staining, the mean background pixel intensity in the negative control section was subtracted from the mean pixel intensity of the VEGF-stained section.

For MVD analysis, the formalin-fixed paraffin-embedded tumors were sectioned (4 µm), dewaxed, and rehydrated. CD31 staining and MVD analysis were carried out as previously reported [32]. Antigen retrieval was done in DAKO buffer S1699 at 121°C for one cycle in a 2100 Retriever Pressure Cooker (PickCell Laboratories, Amsterdam, the Netherlands). All incubations were done at room temperature, and all washes were done with TBST (100 mM Tris pH 7.4, 150 mM NaCl, 0.05% Tween 20). Endogenous biotin was blocked with avidin-biotin block (X0590; DAKO, Ely, UK). Sections were blocked with 5% rabbit serum (DAKO) in TBST for 20 minutes and then incubated in a 1:50 dilution of CD31 antibody (sc-1506) in serum block for 1 hour before washing. Biotinylated rabbit antigoat immunoglobulin (DAKO), diluted 1:200, was then added to the sections for 30 minutes. Vectastain ABC-Elite solution, diluted as instructed in kit, was then added for 30 minutes, and the sections were developed in diaminobenzidine for 10 minutes (Biogenex, San Ramon, CA) and counterstained weakly with Carazzi hematoxylin. MVD analysis was done blinded using an Automated Cellular Imaging System (ACIS; ChromaVision Medical Systems, Inc, San Juan Capistrano, CA). Briefly, each tissue section was scanned into the ACIS at ×10 magnification. Using the ACIS MVD software algorithm, an analysis threshold was set and applied to all

tumors within the study. MVD for each tumor was expressed as the mean number of CD31-positive vascular structures per square millimeter of viable tumor.

For apoptosis analysis, cleaved caspase-3 (CC3) rabbit polyclonal antibodies (Cell Signaling Technology, Danvers, MA) were used followed by a one-step horseradish peroxidase–labeled polymer method (Envision; DAKO). Sections were counterstained with Carazzi hematoxylin. CC3-positive staining was expressed as the percent of nuclei with positive immunostaining.

Statistical Analysis

The nonparametric Wilcoxon matched-pair signed-rank test was used to compare the changes of CT perfusion parameters (BF, BV, MTT, and PS) and TV before and after treatment in nonhypovascular and hypovascular tumors as well as the "combined" group (disregarding vascularity). The Mann-Whitney U test was used to compare the percentage changes of CT perfusion parameters and TV, intensity of VEGF expression, MVD, and percentage CC3 of vehicle- *versus* vandetanib-treated rats in all three groups of tumors. Significance was declared at $P < .05$.

Results

All rats tolerated the anesthesia, DCE-CT scanning, and both vandetanib and vehicle treatments well.

Effects of Vandetanib Treatment on Tumor Perfusion Parameters

Mean tumor BF, BV, MTT, and PS at baseline (before treatment) and at 24 hours (2 hours after the second dose of vandetanib or vehicle) in all groups are shown in Table 1.

Vandetanib reduced tumor BF and BV significantly but not MTT or PS compared with before treatment ($P < .05$), whereas vehicle treatment had no significant effects on any of the perfusion parameters. Subgroup analyses show that the general trend of reduced tumor BF and BV with vandetanib treatment were maintained in both hypovascular and nonhypovascular tumors, but only the reduction of BV in nonhypovascular tumors reached significance. The effects of vandetanib on each perfusion parameter were also investigated as percentage changes relative to baseline values. In the nonhypovascular group, marked percentage reductions of both tumor BF (–21.4% ± 25.5%) and BV (–23.8% ± 20.9%) were observed in vandetanib-treated rats compared with percentage increases in tumor BF (+18.6% ± 19.3%) and BV (+50.7% ± 32.3%) in the vehicle-treated rats (both $P < .05$; Table 2 and Figure 1), but the percentage changes in MTT and PS were not significantly different between vandetanib- and vehicle-treated rats (Table 2 and Figures 1 and 2). In the combined group including both nonhypovascular and hypovascular tumors, only the percent-

age decrease in BV was significantly different between vandetanib- and vehicle-treated rats (–15.5% ± 22.9% *vs* +23.3% ± 36.8%, $P < .01$; Table 2 and Figure 3) but not percentage changes in BF, MTT, or PS (Table 2 and Figure 3). For the hypovascular group, the percentage changes in all perfusion parameters (BF, BV, MTT, and PS) did not differ significantly between vandetanib- and vehicle-treated rats ($P > .05$; Table 2 and Figure 4).

Figures 2 and 5 illustrate CT perfusion parametric maps of representative nonhypovascular and hypovascular tumors, respectively, before and after vandetanib or vehicle treatment. The nonhypovascular tumors had relatively uniform BF and BV throughout the tumor. After vehicle treatment of these tumors, there were notable increases in BF and BV, particularly in a number of foci, within the tumor region (Figure 2, *BF and BV panels of vehicle control*; *arrows*), suggesting that new microvascular foci with enhanced BF and BV activities had developed during 24 hours in vehicle-treated animals. In contrast, after vandetanib treatment, BF and BV maps in nonhypovascular tumors show notable decrease of these parameters (Figure 2, *BF and BV panels of vandetanib treatment*). Of interest, there was a suggestion that these effects of vandetanib treatment were apparent both within the LoVo tumor tissue and adjacent blood vessels (Figure 2, *BF and BV panels of vandetanib treatment*; *arrows and dotted arrows*), although effects in nontumor tissue were not quantified in the present study. The hypovascular tumors had a highly vascular rim, and within, it both BF and BV were much lower than the rim (Figure 5). Both vandetanib and vehicle treatments did not affect either tumor BF or BV (Figure 5).

The distributions of BF and BV within a vehicle-treated nonhypovascular tumor are summarized as normalized histograms in Figure 6, *A* and *C*, whereas those for a vandetanib-treated nonhypovascular tumor are shown as Figure 6, *B* and *D*. For the vehicle-treated nonhypovascular tumor, both tumor BF and BV distributions shifted to the right (higher values) after vehicle treatment compared with those before treatment, graphically showing increases in both BF and BV in the tumor within 24 hours (Figure 6, *A* and *C*). The corresponding normalized histograms of tumor BF and BV in the vandetanib-treated nonhypovascular tumor were left-shifted relative to before treatment, demonstrating that both tumor BF and BV were remarkably inhibited within 24 hours of treatment with vandetanib (Figure 6, *B* and *D*). In the hypovascular tumor, however, no marked changes in both tumor BF and BV distributions were found after 24 hours of treatment with vehicle or vandetanib (Figure 7).

Effects of Vandetanib Treatment on Tumor Growth, VEGF Expression, MVD, and Apoptosis

We also investigated whether vandetanib treatment was associated with other tumor responses such as tumor growth inhibition, tumor cell

Table 1. Mean Tumor BF, BV, MTT, and PS Parameters and TV before (at Baseline, 0 hour) and after Treatment (24 hours) in Vandetanib- or Vehicle-Treated Nonhypovascular and Hypovascular Tumors and All (Combined) Tumors at Week 3 to 4 after Implantation with LoVo Tumor Cells in Nude Rats.

Treatment	Group	BF (ml/min per 100 g)		BV (ml/100 g)		MTT (seconds)		PS (ml/min per 100 g)		TV (mm^3)	
		Before	After	Before	After	Before	After	Before	After	Before	After
Vandetanib	Nonhypovascular ($n = 5$)	86.2 ± 24.9	66.2 ± 24.4	5.4 ± 1.3	4.0* ± 1.1	3.9 ± 8.6	3.8 ± 0.6	22.7 ± 12.0	20.9 ± 11.3	376 ± 126	334 ± 125
	Hypovascular ($n = 8$)	59.9 ± 16.6	53.0 ± 16.0	4.4 ± 1.4	3.8 ± 1.2	4.4 ± 0.5	4.3 ± 0.2	15.1 ± 5.3	14.1 ± 3.0	887 ± 513	855 ± 542
	Combined ($n = 13$)	70.0 ± 23.3	58.1* ± 19.8	4.7 ± 1.4	3.9* ± 1.1	4.2 ± 0.7	4.1 ± 0.5	18.1 ± 8.9	16.7 ± 7.7	691 ± 475	655 ± 497
Vehicle	Nonhypovascular ($n = 4$)	52.1 ± 6.5	61.2 ± 8.0	3.2 ± 0.4	4.7 ± 0.4	3.8 ± 0.8	4.7 ± 0.3	19.2 ± 5.9	16.1 ± 5.0	563 ± 265	550 ± 272
	Hypovascular ($n = 4$)	58.6 ± 18.6	50.0 ± 4.4	4.6 ± 1.3	4.4 ± 1.2	4.7 ± 0.4	5.2 ± 0.9	14.5 ± 4.6	14.8 ± 2.9	744 ± 344	778 ± 483
	Combined ($n = 8$)	55.3 ± 13.4	55.6 ± 8.5	3.9 ± 1.2	4.5 ± 0.8	4.3 ± 0.8	4.9 ± 0.7	16.9 ± 5.5	15.4 ± 3.9	653 ± 300	663 ± 383

Values are mean ± SD.
*Significantly different from before treatment ($P < .05$) as determined by the Wilcoxon matched-pair signed-rank test.

Table 2. Average Percentage Changes (%) in Mean Tumor BF (ml/min per 100 g), BV (ml/100 g), MTT (seconds), PS (ml/min per 100 g), and TV (mm³) Relative to Baseline Values Shown in Table 1 and Average Immunohistochemical End Points for VEGF Expression (Mean Pixel Intensity), MVD (Microvessel Number/mm²), and Apoptosis (CC3-Positive Nuclei/Total Nuclei × 100 [%]) after Treatment with Vandetanib or Vehicle in Nonhypovascular, Hypovascular, and All (Combined) Tumors at 3 to 4 Weeks After Implantation with LoVo Tumor Cells in Nude Rats.

Group	Treatment	BF	BV	MTT	PS	TV	VEGF	MVD	Apoptosis
Nonhypovascular	Vandetanib (n = 5)	**−21.37*** ± 25.5	**−23.78*** ± 20.9	**−0.93** ± 13.2	**−3.28** ± 36.6	**−10.92** ± 11.7	**34.47** ± 10.8	**107.40** ± 38.8	**3.52** ± 0.8
	Vehicle (n = 4)	**18.56** ± 19.3	**50.67** ± 32.3	**28.95** ± 32.5	**−10.45** ± 43.5	**−3.78** ± 7.6	**30.91** ± 3.3	**88.58** ± 46.3	**3.53** ± 1.2
Hypovascular	Vandetanib (n = 8)	**−10.38** ± 24.1	**−10.31** ± 23.9	**0.15** ± 10.1	**1.82** ± 37.7	**−5.49** ± 15.8	**29.51** ± 8.3	**55.23** ± 16.5	**3.59** ± 0.5
	Vehicle (n = 4)	**−10.04** ± 19.8	**−4.03** ± 11.2	**9.99** ± 23.7	**5.30** ± 15.3	**3.13** ± 23.8	**30.03** ± 8.5	**47.96** ± 20.5	**2.66** ± 0.7
Combined	Vandetanib (n = 13)	**−14.61** ± 24.3	**−15.50†** ± 22.9	**−0.26** ± 10.8	**−0.14** ± 35.8	**−7.59** ± 14.1	**31.42** ± 9.2	**74.20** ± 36.2	**3.56** ± 0.6
	Vehicle (n = 8)	**4.27** ± 23.7	**23.30** ± 36.8	**19.47** ± 28.2	**−2.57** ± 31.3	**−0.32** ± 16.8	**30.47** ± 6.0	**68.27** ± 39.0	**3.10** ± 1.0

Values are presented as mean ± SD.
*P ≤ .05, different from the relative change in the vehicle-treated rats as determined by the Mann-Whitney U test.
†P < .01, different from the relative change in the vehicle-treated rats as determined by the Mann-Whitney U test.

death, changes in MVD, or VEGF protein expression during the 24-hour time frame of the study. As shown in Table 1, before treatment, the average TV of vandetanib-treated rats was not significantly different from that of vehicle-treated groups in all three groups (Table 1, *TV in each combined group of vandetanib or vehicle treatment, P > .05*). Before treatment, nonhypovascular tumors were smaller than pretreatment hypovascular tumors (average TVs 459 ± 210 mm³ *vs* 840 ± 452 mm³, respectively, P < .05; data not shown, but refer to Table 1). In addition, there was no significant difference in TVs before and after either vehicle or vandetanib treatment in all three groups.

No significant differences were found in VEGF protein expression (mean staining intensity), MVD (vessel no./mm²), or tumor apoptosis (CC3-positive nuclei/total nuclei × 100 [%]) at 24 hours after treatment between vandetanib- and vehicle-treated animals in all three groups (P ≫ .05; Table 2 and Figures 1, 3, and 4).

Plasma Concentration of Vandetanib

The mean plasma drug concentration in animals sampled 2 hours after the second of two, 22 hours apart, oral doses of vandetanib (50 mg/kg each dose) was 1231 ± 337 ng/ml, whereas no vandetanib was detected in the vehicle-treated controls.

Discussion

The effect of vandetanib has previously been investigated using histology, immunohistochemistry, and tumor size measurements in both preclinical and clinical studies [7,8,33]. For *in vivo* studies, DCE-MRI has been used in both animals and humans to explore the effects of vandetanib on tumor vasculature [34,35]. In the current work, we report on the use of DCE-CT to evaluate the effects of vandetanib on the vasculature in the LoVo human colon tumor xenograft model in nude rats.
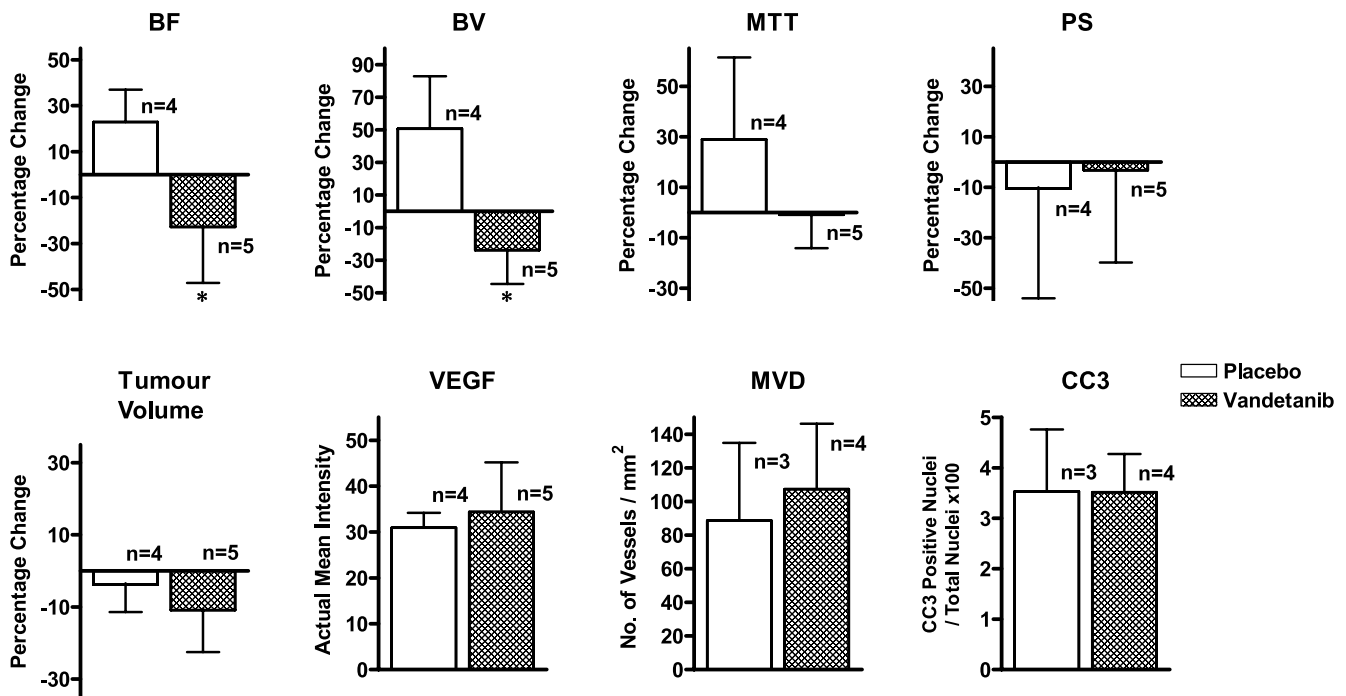
Values are shown as mean ± SD.
*P ≤ .05, different from the vehicle-treated rats as determined by the Mann-Whitney U test.

Figure 1. Bar graph plots of data from nonhypovascular tumors shown in Table 2. The numbers of animals treated with vehicle (open bar) and vandetanib (hatched bar) are shown. Values are shown as mean ±SD. *P ≤ .05, different from the vehicle-treated rats as determined by the Mann-Whitney U test.
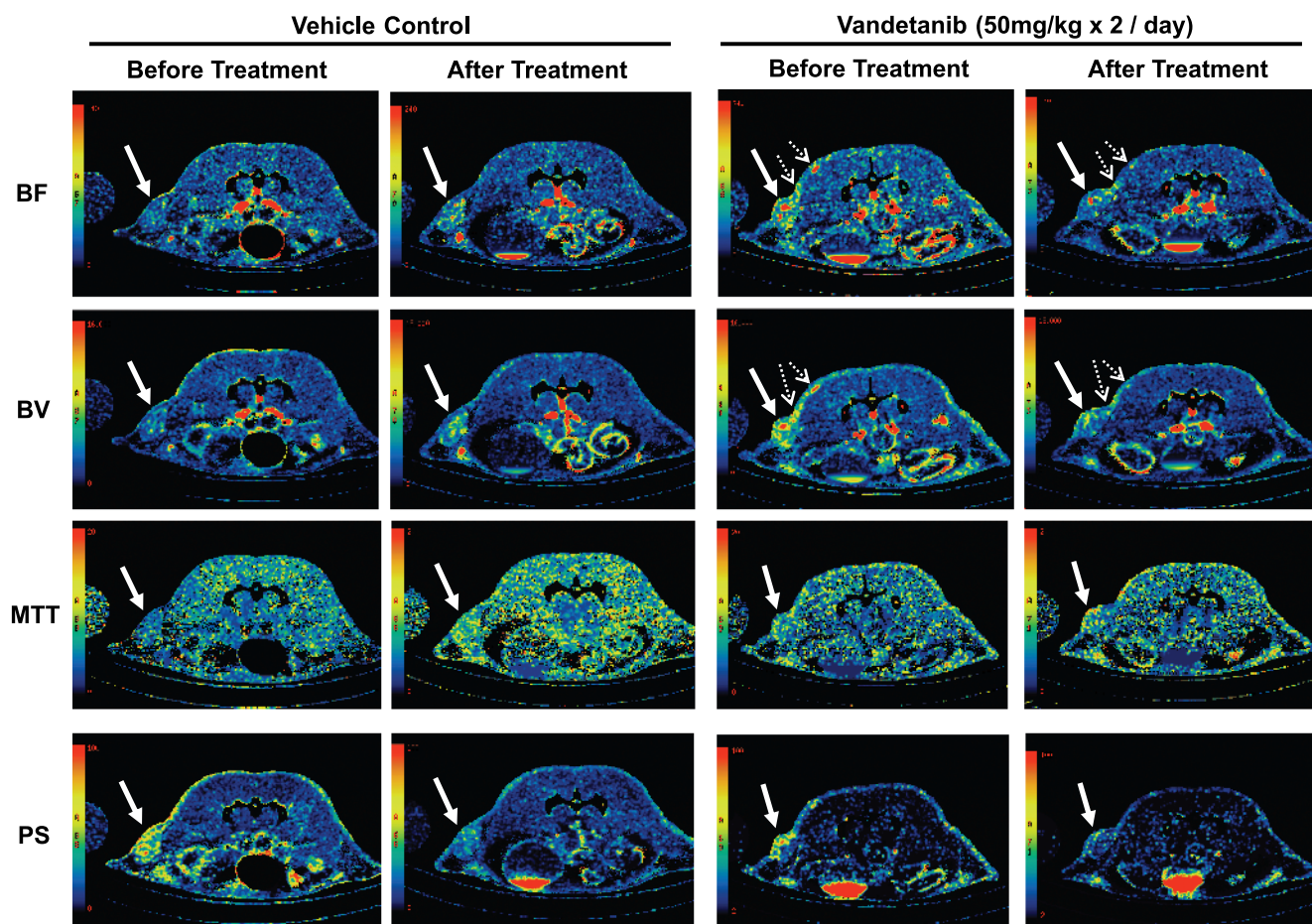
Figure 2. Representative BF, BV, MTT, and PS maps of a transaxial section through the tumor of one vehicle- and one vandetanib-treated nonhypovascular tumor before and after treatment. In the BF, BV, MTT, and PS maps, values from 0 to 240 ml/min per 100 g, from 0 to 16 ml/100 g, from 0 to 20 seconds, and from 0 to 100 ml/min per 100 g, respectively, are coded according to the rainbow color scale. The parametric maps, in particular BF and BV maps, show the level of angiogenic activities in the tumor and adjacent tissue as indicated by solid and dotted arrows respectively.

The oral dose of vandetanib in the present study was selected to achieve plasma drug levels similar to the steady-state plasma levels achieved in clinical trials with 300 mg of vandetanib daily dosing [35]. This was confirmed by measurement of the plasma drug level at 2 hours after the second of two, 22 hours apart, oral doses of vandetanib.

Our study with the LoVo xenograft model showed that vandetanib treatment led to a significant reduction (within 24 hours) of tumor BF and BV. In contrast, in vehicle-treated animals, both tumor BF and BV showed a trend of increase during the experiment. When percentage changes in BF and BV relative to baseline were examined, nonhypovascular tumors showed significant differences between vandetanib and vehicle treatment, whereas hypovascular tumors did not. Similar to previous studies, we found that hypovascular tumors are significantly larger in size than nonhypovascular tumor [36,37]. Furthermore, there is evidence that maturation of vessels is a function of tumor size [38]. In view of these prior results, our study suggests that the difference in response of nonhypovascular versus hypovascular tumors to vandetanib may be related to the differential maturation of tumor vessels in the two types of tumors. It is known that mature (differentiated) vessels are covered with pericytes, which make them resistant to VEGF inhibition, whereas immature (undifferentiated) vessels have less pericyte coverage, and hence, the ECs are more sensitive to anti-VEGF treatment [38,39]. Thus, the therapeutic effect of antiangiogenic agents may be dependent on the rel-

ative proportion of mature versus immature vessels in the tumor [40]. Our study suggests that the vascularity of the tumor may be a surrogate marker for vessel maturity, but this postulate needs to be further investigated in a larger study with immunohistopatholgic correlation.

Of interest, our data also suggest that there was a trend for tumor MTT to decrease or stabilize in vandetanib-treated rats and to increase in vehicle-treated rats (Table 2 and Figures 1, 3, and 4). MTT measures the time for blood to traverse the microcirculation [23] and therefore is directly related to interstitial fluid pressure (IFP) in tumors [41]. Tumor vessels are structurally and functionally abnormal: leaky, tortuous, dilated, saccular, and eccentrically altered [42]. This leakiness of tumor vessels can lead to extravasation of plasma proteins and fluid, producing elevated IFP within tumors [42,43], which is a hallmark of solid tumors. After vandetanib treatment, the stabilized IFP, inferred from the MTT data, may be a result of vascular normalization acting on a subset of tumor blood vessels and would be expected to transiently improve tumor oxygenation thereby potentially limiting the utility of immunohistochemically associated markers with hypoxia (e.g., VEGF expression), tumor cell death (e.g., CC3), or tumor cell proliferation (e.g., Ki67). McCarty et al. [9] reported a striking observation in an orthotopic model of human gastric cancer in a nude mouse, whereby after vandetanib treatment for 23 days, remaining tumor vessels had a three-fold increase in pericyte coverage compared with the control
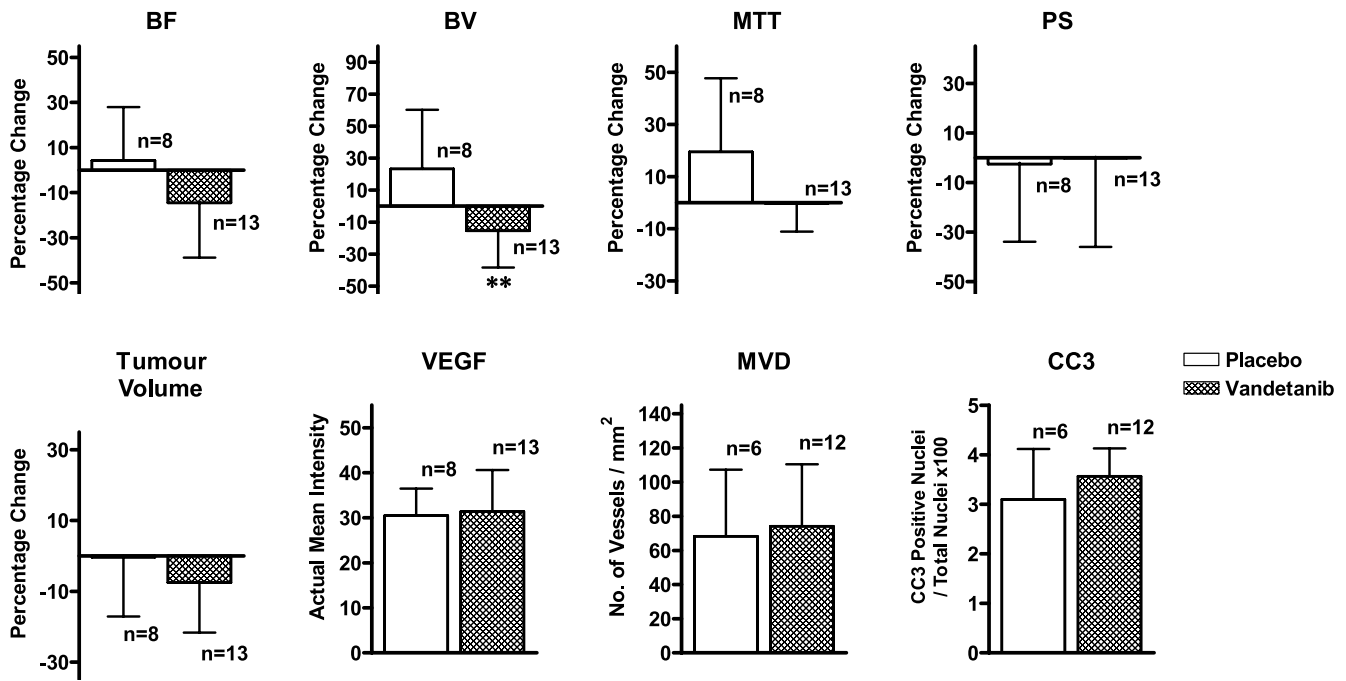
Values are shown as mean $\pm$ SD.

**$**P < .01$, significantly different from the vehicle-treated rats as determined by the Mann-Whitney U test.

Figure 3. Bar graph plots of data from all tumors (combined) in Table 2. The numbers of animals treated with vehicle (open bar) and vande-tanib (hatched bar) are shown. Values are shown as mean $\pm$SD. *$P \leq .01$, different from the vehicle-treated rats as determined by the Mann-Whitney U test.
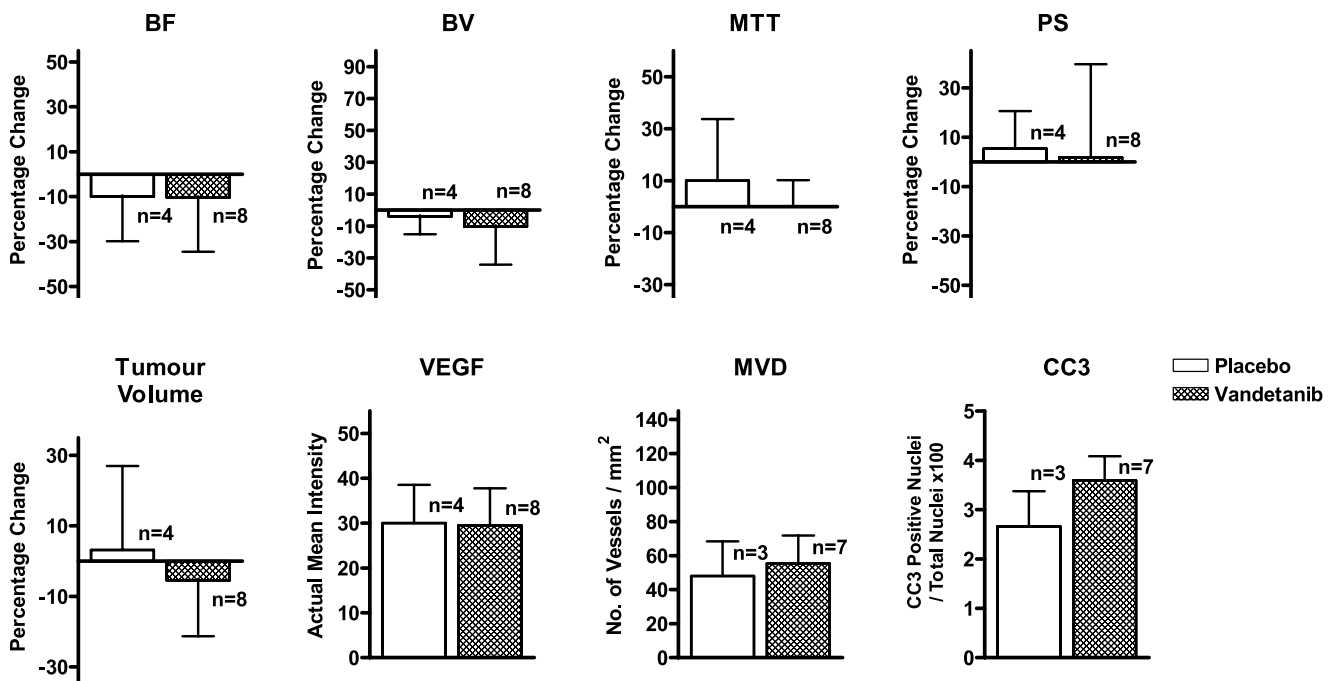
Values are shown as mean $\pm$ SD.

Figure 4. Bar graph plots of data from hypovascular tumors shown in Table 2. The numbers of animals treated with vehicle (open bar) and vandetanib (hatched bar) are shown. Values are shown as mean $\pm$SD.
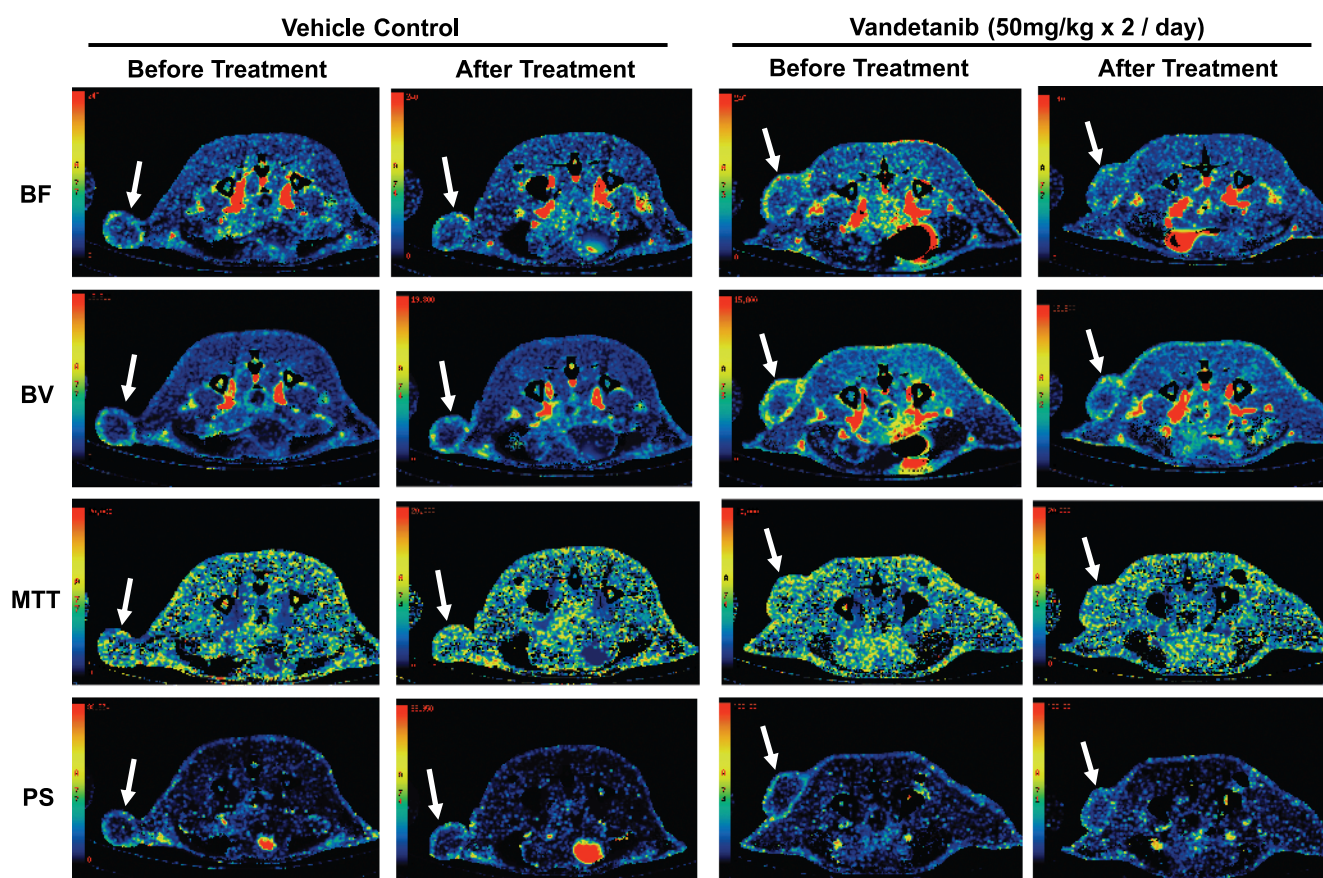
Figure 5. Representative BF, BV, MTT, and PS maps of a transaxial section through the tumor of one vehicle- and one vandetanib-treated hypovascular tumor before and after treatment. In the BF, BV, MTT, and PS maps, values from 0 to 240 ml/min per 100 g, from 0 to 16 ml/100 g, from 0 to 20 seconds, and from 0 to 100 ml/min per 100 g, respectively, are coded according to the rainbow color scale. The parametric maps, in particular BF and BV maps, show the level of angiogenic activities in the tumors as indicated by the solid arrow.

group, supporting the hypothesis of vascular normalization induced by vandetanib. Additional experiments with longer treatment durations would be required to evaluate the dynamics of vascular normalization in the LoVo tumor model used in the present study and could provide important information for determining the optimal dosing schedule of vandetanib in combination with standard therapies such as chemotherapy and radiotherapy [43].

There were no significant changes in PS after treatment. These results were similar to those obtained by Willett et al. [44] who showed, also by using DCE-CT, that a single infusion of the VEGF-specific antibody, bevacizumab decreased tumor perfusion and vascular volume, but a change in PS was below the detection limit with DCE-CT in patients with rectal cancer. This null effect of vandetanib on PS in the present study is also similar to the results obtained by Raatschen et al. [45]. They measured PS in MDA MB-435 xenograft tumor using two different molecular weight x-ray contrast (821 vs 66,000 Da). The low–molecular weight contrast is the same as the one used in this study (Omnipaque; GE Healthcare). They found that after one dose of bevacizumab, while PS measured with the high–molecular weight contrast decreased significantly, that measured with the low–molecular weight contrast did not change. Although normal endothelium is impermeable to the high–molecular weight contrast, tumor endothelium is permeable because of the presence of endothelial fenestrations. With antiangiogenic treatment, the endothelial fenestrations are reduced [46], leading to a decrease in PS measured with high–molecular weight agent; however,

although the fenestrations are reduced in size, they are still passable to low–molecular weight contrast, thus PS measured with low–molecular weight contrast will not change. As such, it seems that measurement of PS with high–molecular weight contrast could better reflect the closing of the fenestrations in tumor endothelium by antiangiogenics than low–molecular weight contrast [45]. However, as discussed above, the reduction in the leakage of plasma proteins into the interstitium would lead to a drop in interstitial pressure and a concomitant decrease in MTT. Thus, measurement of MTT with a low–molecular weight as was the case in the present study could also indicate the closing of endothelial fenestrations in the tumor epithelium. MTT assessment is also technique-dependent, depending on the temporal resolution, spatial resolution, and sensitivity.

The complexity and timing of downstream tumor cell responses to the antivascular effects of VEGF signaling inhibitors, together with the sampling variability inherent in tumor biopsies suggest that histologic end points may have only limited utility as effective biomarkers to demonstrate the pharmacodynamic effects of VEGF signaling inhibitors in tumors in the clinic. In rats implanted with FN 13762 tumors in the liver, Kan et al. [47] used DCE-CT to measure tumor perfusion parameters with and without the VEGFR TK inhibitor SU5416. In that study, BF, BV, and PS were significantly higher in SU5416-treated tumors than in control tumors, whereas MVD was significantly lower. These results for SU5416 differed from the present study with vandetanib where tumors experienced a significant decrease in both

BV and BF but no change in MVD or PS. However, compared with the present study, Kan et al. studied tumors in the orthotopic setting rather than subcutaneously, and the tumors were much larger with hypovascular regions. In addition, in that previous study, the DCE-CT was performed at baseline and after 2 weeks of treatment, rather than immediately, as in the present study.

We did not find any significant difference in MVD between vandetanib- and vehicle-treated groups, implying that changes in vascular organization such as MVD are not expected to occur within 24 hours of initiating therapy. However, MVD does not discriminate between functional and nonfunctional tumor blood vessels and may be limited in revealing the immediate effects of VEGF signaling inhibitors [48]. In addition, we did not observe any difference in tumor cell apoptosis or VEGF expression. Increased apoptosis has been reported in preclinical tumor models in response to vandetanib [9,49], although these previous studies evaluated tumor apoptosis after several days or weeks of treatment and not at very early time points (24 hours) as in the present work. VEGF protein expression has been reported to be upregulated in patients treated with VEGF signaling inhibitors, although the mechanisms underlying this effect are not understood [50]. However, we did not see any difference in VEGF expression between vandetanib- and vehicle-treated tumors in this study whether they were hypovascular or not. This could be due to the short duration of treatment (24 hours) used in the present study, high constitutive expression of VEGF through non–hypoxia-regulated pathways [51] and/or vessel normalization transiently improving oxygen delivery despite the overall reduction in tumor BF and BV [42].

Compared with other imaging modalities that can be used to measure tumor perfusion, CT has a number of advantages [23,25]. Firstly, it rivals the ability of PET for kinetic modeling of the uptake of contrast because tissue contrast concentration can be accurately and quantitatively measured. Secondly, it has the highest combination of temporal frequency (~1 Hz) and spatial resolution in dynamic scanning, which permits the accurate characterization of the uptake and washout of contrast agent with submillimeter resolution, in this case 0.18 mm. Thirdly, the arterial input curve can be measured from the same dynamic CT images as the tissue concentration [23], obviating the need for invasive arterial sampling or more complicated postprocessing of image data [52,53]. Fourthly, CT is widely accessible in most hospitals and is not limited to academic or tertiary hospitals. DCE-MRI also offers many of the advantages of DCE-CT without the inconvenience of ionizing radiation or limited coverage. However, the technique is hampered by its complexity and the lack of straightforward relationship between signal intensity and contrast agent concentration, which make the results more difficult to interpret [22,24]. Also, DCE-MRI may not be feasible for some patient groups, especially individuals with kidney failure (because of the risk of nephrogenic systemic fibrosis), those with implanted devices (cardiac pacemakers, prosthetic valves, intracranial aneurismal clips, shrapnel injury), and those with severe claustrophobia [22].

One limitation of DCE-CT as developed in this study for the monitoring of therapy is the relatively high radiation dose, which can be as high as 20 mSv [54]. Although radiation dose is limited in a single DCE-CT study, the accumulated radiation dose from multiple DCE-CT studies to monitor the effect of therapy over time may pose a
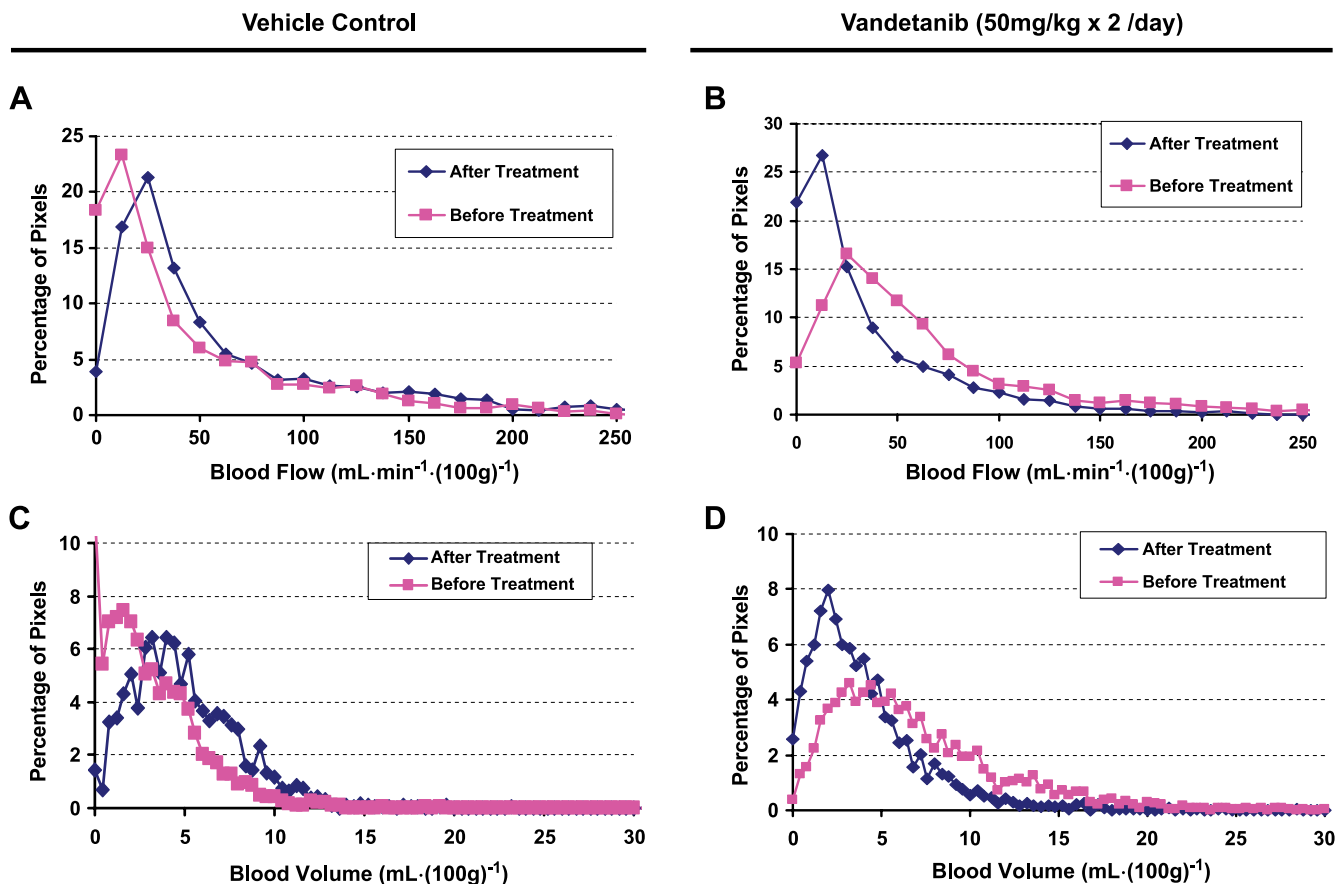

Figure 6. The corresponding normalized whole tumor BF and BV histograms of the nonhypovascular tumors shown in Figure 2 before and after treatment with vehicle (A, C) and vandetanib (B, D).
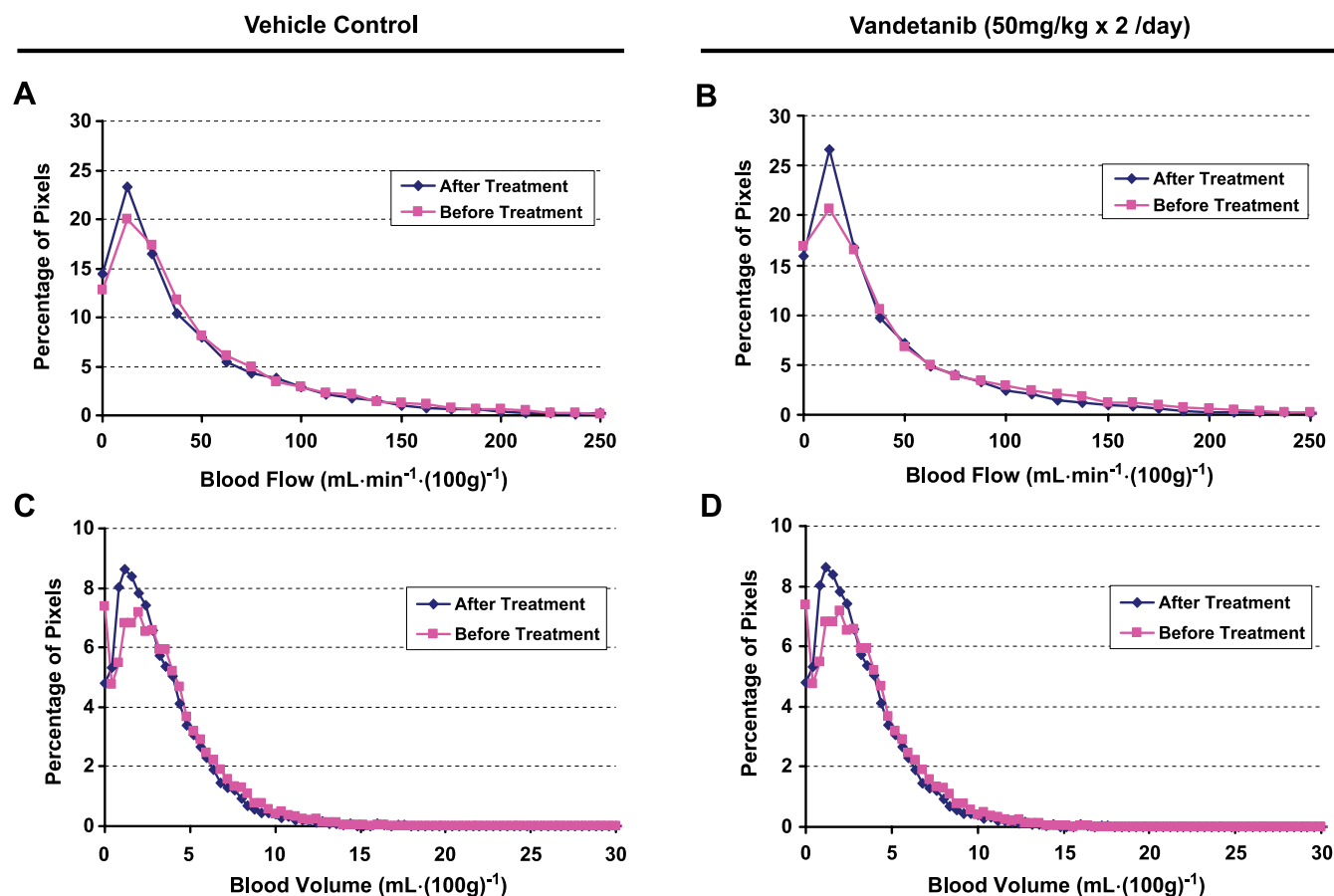
Figure 7. The corresponding normalized whole tumor BF and BV histograms of the hypovascular tumors shown in Figure 5 before and after treatment with vehicle (A, C) and vandetanib (B, D).

concern. However, advances in CT reconstruction techniques, such as the statistical iterative method proposed by Thibault et al. [55], may significantly reduce the radiation dose without sacrificing image quality. The application of these image reconstruction algorithms to DCE-CT is currently under investigation. Another limitation is the contrast-induced nephrotoxicity such that patients with poor renal function (i.e., estimated glomerular filtration rate <30 ml/min) have to be excluded.

In conclusion, our study demonstrated that DCE-CT can detect the immediate effects of vandetanib, given twice orally during 24 hours, on tumor vasculature in the absence of significant effects on TV or histologic markers. As such, DCE-CT has promise for early, noninvasive assessment of vascular response to antiangiogenesis agents in the clinic, in particular, allowing broader clinical utility than more complex functional imaging modalities such as DCE-MRI.

Acknowledgments

References

[1] Folkman J (1971). Tumor angiogenesis: therapeutic implications. *N Engl J Med* **285**, 1182–1186.

[2] Li WW (2000). Tumor angiogenesis: molecular pathology, therapeutic targeting, and imaging. *Acad Radiol* **7**, 800–811.

[3] Carmeliet P (2005). Angiogenesis in life, disease and medicine. *Nature* **438**, 932–936.

[4] Kerbel RS (2008). Tumor angiogenesis. *N Engl J Med* **358**, 2039–2049.

[5] Hicklin DJ and Ellis LM (2005). Role of the vascular endothelial growth factor pathway in tumor growth and angiogenesis. *J Clin Oncol* **23**, 1011–1027.

[6] Folkman J (1995). Seminars in Medicine of the Beth Israel Hospital, Boston. Clinical applications of research on angiogenesis. *N Engl J Med* **333**, 1757–1763.

[7] Ryan AJ and Wedge SR (2005). ZD6474—a novel inhibitor of VEGFR and EGFR tyrosine kinase activity. *Br J Cancer* **92**(suppl 1), S6–S13.

[8] Wedge SR, Ogilvie DJ, Dukes M, Kendrew J, Chester R, Jackson JA, Boffey SJ, Valentine PJ, Curwen JO, Musgrove HL, et al. (2002). ZD6474 inhibits vascular endothelial growth factor signaling, angiogenesis, and tumor growth following oral administration. *Cancer Res* **62**, 4645–4655.

[9] McCarty MF, Wey J, Stoeltzing O, Liu W, Fan F, Bucana C, Mansfield PF, Ryan AJ, and Ellis LM (2004). ZD6474, a vascular endothelial growth factor receptor tyrosine kinase inhibitor with additional activity against epidermal growth factor receptor tyrosine kinase, inhibits orthotopic growth and angiogenesis of gastric cancer. *Mol Cancer Ther* **3**, 1041–1048.

[10] Conrad C, Ischenko I, Kohl G, Wiegand U, Guba M, Yezhelyev M, Ryan AJ, Barge A, Geissler EK, Wedge SR, et al. (2007). Antiangiogenic and antitumor activity of a novel vascular endothelial growth factor receptor-2 tyrosine kinase inhibitor ZD6474 in a metastatic human pancreatic tumor model. *Anticancer Drugs* **18**, 569–579.

[11] Miller AB, Hoogstraten B, Staquet M, and Winkler A (1981). Reporting results of cancer treatment. *Cancer* **47**, 207–214.

[12] Therasse P, Arbuck SG, Eisenhauer EA, Wanders J, Kaplan RS, Rubinstein L, Verweij J, Van Glabbeke M, van Oosterom AT, Christian MC, et al. (2000). New guidelines to evaluate the response to treatment in solid tumors. European Organization for Research and Treatment of Cancer, National Cancer Institute of the United States, National Cancer Institute of Canada. *J Natl Cancer Inst* **92**, 205–216.

[13] Eisenhauer EA, Therasse P, Bogaerts J, Schwartz LH, Sargent D, Ford R, Dancey J, Arbuck S, Gwyther S, Mooney M, et al. (2009). New response evaluation criteria in solid tumours: revised RECIST guideline (version 1.1). *Eur J Cancer* **45**, 228–247.

[14] Weidner N (1995). Intratumor microvessel density as a prognostic factor in cancer. *Am J Pathol* **147**, 9–19.

[15] Weidner N, Semple JP, Welch WR, and Folkman J (1991). Tumor angiogenesis and metastasis—correlation in invasive breast carcinoma. *N Engl J Med* **324**, 1–8.

[16] Ushijima C, Tsukamoto S, Yamazaki K, Yoshino I, Sugio K, and Sugimachi K (2001). High vascularity in the peripheral region of non–small cell lung cancer tissue is associated with tumor progression. *Lung Cancer* **34**, 233–241.

[17] Miles KA and Griffiths MR (2003). Perfusion CT: a worthwhile enhancement? *Br J Radiol* **76**, 220–231.

[18] Goh V, Halligan S, Daley F, Wellsted DM, Guenther T, and Bartram CI (2008). Colorectal tumor vascularity: quantitative assessment with multidetector CT—do tumor perfusion measurements reflect angiogenesis? *Radiology* **249**, 510–517.

[19] Sabir A, Schor-Bardach R, Wilcox CJ, Rahmanuddin S, Atkins MB, Kruskal JB, Signoretti S, Raptopoulos VD, and Goldberg SN (2008). Perfusion MDCT enables early detection of therapeutic response to antiangiogenic therapy. *AJR Am J Roentgenol* **191**, 133–139.

[20] Galbraith SM, Maxwell RJ, Lodge MA, Tozer GM, Wilson J, Taylor NJ, Stirling JJ, Sena L, Padhani AR, and Rustin GJ (2003). Combretastatin A4 phosphate has tumor antivascular activity in rat and man as demonstrated by dynamic magnetic resonance imaging. *J Clin Oncol* **21**, 2831–2842.

[21] Drevs J, Siegert P, Medinger M, Mross K, Strecker R, Zirrgiebel U, Harder J, Blum H, Robertson J, Jurgensmeier JM, et al. (2007). Phase I clinical study of AZD2171, an oral vascular endothelial growth factor signaling inhibitor, in patients with advanced solid tumors. *J Clin Oncol* **25**, 3045–3054.

[22] Turkbey B, Kobayashi H, Ogawa M, Bernardo M, and Choyke PL (2009). Imaging of tumor angiogenesis: functional or targeted? *AJR Am J Roentgenol* **193**, 304–313.

[23] Lee TY, Purdie TG, and Stewart E (2003). CT imaging of angiogenesis. *Q J Nucl Med* **47**, 171–187.

[24] Miles KA, Charnsangavej C, Lee FT, Fishman EK, Horton K, and Lee TY (2000). Application of CT in the investigation of angiogenesis in oncology. *Acad Radiol* **7**, 840–850.

[25] Lee T (2002). Functional CT: physiological models. *Trends Biotechnol* **20**, S3–S10.

[26] Gandhi D, Hoeffner EG, Carlos RC, Case I, and Mukherji SK (2003). Computed tomography perfusion of squamous cell carcinoma of the upper aerodigestive tract. Initial results. *J Comput Assist Tomogr* **27**, 687–693.

[27] Sahani DV, Kalva SP, Hamberg LM, Hahn PF, Willett CG, Saini S, Mueller PR, and Lee TY (2005). Assessing tumor perfusion and treatment response in rectal cancer with multisection CT: initial observations. *Radiology* **234**, 785–792.

[28] Zhu AX, Holalkere NS, Muzikansky A, Horgan K, and Sahani DV (2008). Early antiangiogenic activity of bevacizumab evaluated by computed tomography perfusion scan in patients with advanced hepatocellular carcinoma. *Oncologist* **13**, 120–125.

[29] Petralia G, Preda L, Giugliano G, Jereczek-Fossa BA, Rocca A, D'Andrea G, Holalkere NS, Chiesa F, and Bellomi M (2009). Perfusion computed tomography for monitoring induction chemotherapy in patients with squamous cell carcinoma of the upper aerodigestive tract: correlation between changes in tumor perfusion and tumor volume. *J Comput Assist Tomogr* **33**, 552–559.

[30] Bellomi M, Petralia G, Sonzogni A, Zampino MG, and Rocca A (2007). CT perfusion for the monitoring of neoadjuvant chemotherapy and radiation therapy in rectal carcinoma: initial experience. *Radiology* **244**, 486–493.

[31] Saunders MP, Wilson R, Peeters M, Smith R, Godwood A, Oliver S, and Van Cutsem E (2009). Vandetanib with FOLFIRI in patients with advanced colorectal adenocarcinoma: results from an open-label, multicentre phase I study. *Cancer Chemother Pharmacol* **64**, 665–672.

[32] Smith NR, James NH, Oakley I, Wainwright A, Copley C, Kendrew J, Womersley LM, Jurgensmeier JM, Wedge SR, and Barry ST (2007). Acute pharmacodynamic and antivascular effects of the vascular endothelial growth factor signaling inhibitor AZD2171 in Calu-6 human lung tumor xenografts. *Mol Cancer Ther* **6**, 2198–2208.

[33] de Boer R, Humblet Y, Wolf J, Nogova L, Ruffert K, Milenkova T, Smith R, Godwood A, and Vansteenkiste J (2009). An open-label study of vandetanib with pemetrexed in patients with previously treated non-small-cell lung cancer. *Ann Oncol* **20**, 486–491.

[34] Bradley DP, Tessier JL, Checkley D, Kuribayashi H, Waterton JC, Kendrew J, and Wedge SR (2008). Effects of AZD2171 and vandetanib (ZD6474, Zactima) on haemodynamic variables in an SW620 human colon tumour model: an investigation using dynamic contrast-enhanced MRI and the rapid clearance blood pool contrast agent, P792 (gadomelitol). *NMR Biomed* **21**, 42–52.

[35] Mross K, Fasol U, Frost A, Benkelmann R, Kuhlmann J, Büchert M, Unger C, Blum H, Hennig J, Milenkova TP, et al. (2009). DCE-MRI assessment of the effect of vandetanib on tumor vasculature in patients with advanced colorectal cancer and liver metastases: a randomized phase I study. *J Angiogenes Res* **1**, 1–12.

[36] Sevick EM and Jain RK (1989). Geometric resistance to blood flow in solid tumors perfused *ex vivo*: effects of tumor size and perfusion pressure. *Cancer Res* **49**, 3506–3512.

[37] Gyves JW, Ziessman HA, Ensminger WD, Thrall JH, Niederhuber JE, Keyes JW Jr, and Walker S (1984). Definition of hepatic tumor microcirculation by single photon emission computerized tomography (SPECT). *J Nucl Med* **25**, 972–977.

[38] Gee MS, Procopio WN, Makonnen S, Feldman MD, Yeilding NM, and Lee WM (2003). Tumor vessel development and maturation impose limits on the effectiveness of anti-vascular therapy. *Am J Pathol* **162**, 183–193.

[39] Jain RK (2003). Molecular regulation of vessel maturation. *Nat Med* **9**, 685–693.

[40] Qian CN, Huang D, Wondergem B, and Teh BT (2009). Complexity of tumor vasculature in clear cell renal cell carcinoma. *Cancer* **115**, 2282–2289.

[41] Schumann P, Touzani O, Young AR, Morello R, Baron JC, and MacKenzie ET (1998). Evaluation of the ratio of cerebral blood flow to cerebral blood volume as an index of local cerebral perfusion pressure. *Brain* **121**(pt 7), 1369–1379.

[42] Jain RK (2005). Normalization of tumor vasculature: an emerging concept in antiangiogenic therapy. *Science* **307**, 58–62.

[43] Kerbel RS (2006). Antiangiogenic therapy: a universal chemosensitization strategy for cancer? *Science* **312**, 1171–1175.

[44] Willett CG, Boucher Y, di Tomaso E, Duda DG, Munn LL, Tong RT, Chung DC, Sahani DV, Kalva SP, Kozin SV, et al. (2004). Direct evidence that the VEGF-specific antibody bevacizumab has antivascular effects in human rectal cancer. *Nat Med* **10**, 145–147.

[45] Raatschen HJ, Fu Y, Brasch RC, Pietsch H, Shames DM, and Yeh BM (2009). *In vivo* monitoring of angiogenesis inhibitory treatment effects by dynamic contrast-enhanced computed tomography in a xenograft tumor model. *Invest Radiol* **44**, 265–270.

[46] Inai T, Mancuso M, Hashizume H, Baffert F, Haskell A, Baluk P, Hu-Lowe DD, Shalinsky DR, Thurston G, Yancopoulos GD, et al. (2004). Inhibition of vascular endothelial growth factor (VEGF) signaling in cancer causes loss of endothelial fenestrations, regression of tumor vessels, and appearance of basement membrane ghosts. *Am J Pathol* **165**, 35–52.

[47] Kan Z, Phongkitkarun S, Kobayashi S, Tang Y, Ellis LM, Lee TY, and Charnsangavej C (2005). Functional CT for quantifying tumor perfusion in antiangiogenic therapy in a rat model. *Radiology* **237**, 151–158.

[48] Hlatky L, Hahnfeldt P, and Folkman J (2002). Clinical application of antiangiogenic therapy: microvessel density, what it does and doesn't tell us. *J Natl Cancer Inst* **94**, 883–893.

[49] Wu W, Onn A, Isobe T, Itasaka S, Langley RR, Shitani T, Shibuya K, Komaki R, Ryan AJ, Fidler IJ, et al. (2007). Targeted therapy of orthotopic human lung cancer by combined vascular endothelial growth factor and epidermal growth factor receptor signaling blockade. *Mol Cancer Ther* **6**, 471–483.

[50] Jain RK, Duda DG, Clark JW, and Loeffler JS (2006). Lessons from phase III clinical trials on anti-VEGF therapy for cancer. *Nat Clin Pract Oncol* **3**, 24–40.

[51] Kerbel RS (2005). Therapeutic implications of intrinsic or induced angiogenic growth factor redundancy in tumors revealed. *Cancer Cell* **8**, 269–271.

[52] Naganawa M, Kimura Y, Yano J, Mishina M, Yanagisawa M, Ishii K, Oda K, and Ishiwata K (2008). Robust estimation of the arterial input function for Logan plots using an intersectional searching algorithm and clustering in positron emission tomography for neuroreceptor imaging. *Neuroimage* **40**, 26–34.

[53] Guo H, Renaut RA, and Chen K (2007). An input function estimation method for FDG-PET human brain studies. *Nucl Med Biol* **34**, 483–492.

[54] Boone JM, Velazquez O, and Cherry SR (2004). Small-animal X-ray dose from micro-CT. *Mol Imaging* **3**, 149–158.

[55] Thibault JB, Sauer KD, Bouman CA, and Hsieh J (2007). A three-dimensional statistical approach to improved image quality for multislice helical CT. *Med Phys* **34**, 4526–4544.